JVST B
Journal of Vacuum Science & Technology B

Fusion data analysis of imaging data of hydrogen-permeated steel obtained by complementary methods

Cite as: J. Vac. Sci. Technol. B **38**, 034007 (2020); https://doi.org/10.1116/6.0000009
Submitted: 21 January 2020 . Accepted: 23 March 2020 . Published Online: 14 April 2020

Tomomi Akiyama, Naoya Miyauchi, Akiko N. Itakura, Takayuki Yamagishi, and Satoka Aoyagi

COLLECTIONS

Paper published as part of the special topic on Special Topic Collection on Secondary Ion Mass Spectrometry (SIMS)

View Online Export Citation CrossMark

ARTICLES YOU MAY BE INTERESTED IN

Improvement of ionization yield in sputtered neutral mass spectrometry using pulsed infrared and ultraviolet lasers
Journal of Vacuum Science & Technology B **38**, 034011 (2020); https://doi.org/10.1116/6.0000088

Structural analysis of organic ultrathin-layer by using Ar-gas-cluster ion beam sputter collecting method
Journal of Vacuum Science & Technology B **38**, 034003 (2020); https://doi.org/10.1116/6.0000102

Absorption, discharge, and internal partitioning behavior of hydrogen in the tantalum and tantalum oxide system investigated by in situ oxidation SIMS and ab initio calculations
Journal of Vacuum Science & Technology B **38**, 034008 (2020); https://doi.org/10.1116/6.0000100

© 2020 Author(s).

JVST B
Journal of Vacuum Science & Technology B

ARTICLE

avs.scitation.org/journal/jvb

Fusion data analysis of imaging data of hydrogen-permeated steel obtained by complementary methods

Cite as: J. Vac. Sci. Technol. B 38, 034007 (2020); doi: 10.1116/6.0000009
Submitted: 21 January 2020 · Accepted: 23 March 2020 ·
Published Online: 14 April 2020

View Online Export Citation CrossMark

Tomomi Akiyama,[1] Naoya Miyauchi,[2] Akiko N. Itakura,[2] Takayuki Yamagishi,[1] and Satoka Aoyagi[1,a)]

AFFILIATIONS

[1]Faculty of Science and Technology, Seikei University, 3-3-1 Kichijoji-Kitamachi, Musashino-shi, Tokyo 180-8633, Japan
[2]Surface Physics and Characterization Group, National Institute for Materials Science, 1-2-1 Sengen, Tsukuba, Ibaraki 305-0047, Japan

Note: This paper is part of the 2020 Special Topic Collection on Secondary Ion Mass Spectrometry, SIMS.
[a)]**Electronic mail:** aoyagi@st.seikei.ac.jp

ABSTRACT

Chemical imaging, such as mass imaging, provides a distribution image of a particular matter and is crucial for analyzing the chemical and physical mechanisms of a sample. However, methods that provide molecular or elemental distribution do not always have sufficiently high spatial resolution to evaluate the nanosized structures in a sample. To address this issue, a multimodal data analysis method was developed by integrating the obtained low spatial resolution chemical images with complementary methods. In this study, the hydrogen distribution of a steel sample was measured using electron stimulated desorption (ESD) and scanning electron microscopy (SEM). ESD provided the time-course images of hydrogen distribution in the steel sample, whereas SEM provided the outline of the steel sample structure. The multimodal images of the same sample were fused, and then all the data were analyzed together to extract detailed physical and chemical information that cannot be observed by only one of the methods. The alignment of the images obtained using different methods was evaluated based on the minimization of each pixel subtraction. Three different data analysis methods, principal component analysis, least absolute shrinkage and selection operator, and autoencoder, are applied to the image fusion dataset of the ESD image and SEM images to help elucidate the hydrogen permeation behavior through the steel structure.

© 2020 Author(s). All article content, except where otherwise noted, is licensed under a Creative Commons Attribution (CC BY) license (http://creativecommons.org/licenses/by/4.0/). https://doi.org/10.1116/6.0000009

I. INTRODUCTION

Multiple analysis methods such as molecular or elemental mapping and crystal structure analysis are often required to characterize samples that have complex structures and features. The results from different methods occasionally have different data formats, which make it difficult to interpret. Therefore, it is necessary to develop a data analysis method for the evaluation of multimodal datasets. In our previous study on multimodal data,[1] time-of-flight secondary ion mass spectrometry (TOF-SIMS) data containing chemical images with a resolution of several hundred nanometers and microscope image data were fused. The fusion data were analyzed via principal component analysis (PCA) to obtain PCA score images with a higher spatial resolution and PCA loadings with detailed spectrum information. The PCA loadings of the image fusion data were almost the same as those of the TOF-SIMS data, which implies that the chemical information provided by TOF-SIMS is preserved after the fusion of image data with other measurement method data. The analysis of the image fusion data provides more information than that obtained using one single analysis method. In this study, modified image data fusion procedures were developed, and the image fusion dataset was analyzed using PCA, the least absolute shrinkage and selection operator (LASSO), and autoencoder. LASSO, which is a sparse modeling method,[2] was employed to directly search for chemical images similar to a higher lateral resolution microscopic image, while autoencoder, an unsupervised artificial neural network method,[3]

© Author(s) 2020

was used to classify fusion data. Autoencoder is capable of classifying fusion datasets into more detailed categories, as compared to PCA. The data analysis results of individual method data were compared with that of the fusion data to evaluate the effects of image data fusion.

Images obtained using various surface analysis techniques can be integrated as one dataset. In this study, the time-course images of hydrogen distribution in a steel sample obtained using electron stimulated desorption (ESD),[4] which is one of the desorption induced by electronic transition[5] methods, and the same sample image obtained using scanning electron microscopy (SEM) were fused as one dataset. It is important to observe hydrogen adsorption and permeation through the crystals in the steel sample to understand the hydrogen embrittlement of steels,[6,7] although the observation of hydrogen, which is the lightest element, is generally difficult. ESD provides a two-dimensional distribution of hydrogen adsorbed on the steel surface by scanning an electron beam.[8] However, the spatial resolution of ESD is insufficient for observing crystal structures in steel samples. In contrast, SEM (Ref. 9) provides nanoscale distribution images and detailed crystal structures. Therefore, an image data fusion method for the multimodal data of a hydrogen flowing steel sample obtained via ESD and SEM images was developed to obtain hydrogen specific distributions with sufficiently high spatial resolution for identifying the differences between crystal structures.

II. EXPERIMENT

A. Electron stimulated desorption

Stainless steel (SUS304) with dislocation was used as the sample for measuring the time-course images of hydrogen distribution with an ESD system built in the SEM (JAMP10, JEOL, Tokyo) equipment.[7] The sample SUS304 steel has an austenitic phase before cold-working, and a part of austenite grains is transformed into martensite by cold-working (cold-rolled 10%). Hydrogen gas (deuterium 99.96%) at 1 atm was supplied to the backside of the sample membrane (steel with a thickness of 100 μm), which penetrates the sample and reaches the surface. The ESD pattern of hydrogen reflects the density of dislocations in martensite caused by lathe processing on the austenite steel surface. The electron energies used in SEM and ESD were 3 and 1 keV, respectively.

The measurement area of the sample SUS304 steel was 330 μm (vertical) $\times$ 520 μm (horizontal), and the size of original pixels for the whole measurement area was 2048 $\times$ 2048 pixels. The pixel size of ESD hydrogen images was reduced to 64 $\times$ 64 pixels to increase the number of ions per pixel. The time-course images of hydrogen distribution and an SEM image were used for image data fusion. The resolution of the SEM was 2000 $\times$ 2000 pixels, whereas the resolution of hydrogen image data was set to 64 $\times$ 64 pixels. A total of 13 ESD hydrogen images were obtained at the interval of 5 h ranging from 0 to 65 h.

B. Image data fusion

The image fusion programs were written in MATLAB (Mathworks, MA, USA). An SEM image and ESD total image (accumulating signals for 65 h) of almost the same area of the same sample were used for the image data fusion alignment. The measured area of the sample was 330 μm (vertical) $\times$ 520 μm (horizontal). Because these two images were slightly different, the SEM image was rotated several degrees to align with the ESD image. Next, the SEM image was trimmed so that the rotated SEM image was almost perfectly aligned with the ESD image. If necessary, the ESD image can also be trimmed to align with the SEM image because the trimmed SEM image could sometimes be smaller than the ESD image. Subsequently, the resolutions of the trimmed SEM and ESD images were resized to 250 $\times$ 250 pixels. The pixel size was changed using MATLAB (Mathworks, Inc., Natick, MA, USA) command, imresize. Finally, the intensity difference at each pixel of the SEM and ESD images was calculated, and the total intensity difference was obtained. If both images were exactly the same, the total intensity difference should be zero. Thus, the rotation and trimming procedures were repeated until the smallest total difference was obtained. This was the final image that had the smallest total intensity difference at every pixel.

C. Principal component analysis

Autoscaling (the dataset is initially mean-centered and subsequently divided by the standard deviation) was applied to the image fusion data before PCA. PLS Toolbox (Eigenvector Research Inc., WA, USA)[10] working on MATLAB (Mathworks, MA, USA) was used for PCA. The intensity of the SEM or the fluorescent microscopic image was added as a new variable to the variables of the ESD hydrogen time-course image data. PCA was performed using the matrix data of the ESD and the fusion data of ESD and SEM.

D. Least absolute shrinkage and selection operator

LASSO (Ref. 2) was used to identify appropriate solutions by minimizing the error between a target and solutions. Moreover, the L_1 norm (sum of the absolute values of the intensity) of the solutions was used. The solutions were obtained by minimizing E, as expressed in the following equation:

$$E = \|\boldsymbol{Y} - \boldsymbol{A}\boldsymbol{x}\|^2 + \lambda \sum |x_i|. \quad (1)$$

In this equation, the vector $\boldsymbol{Y}$ is the target. The vector $\boldsymbol{Y}$ corresponds to the SEM image that is exactly aligned with the target data $\boldsymbol{A}$, the ESD hydrogen time-course images. The vector x, which provides the minimum value of E in Eq. (1), was identified using LASSO.[2]

The first term in the right-hand side of Eq. (1) is the square error between $\boldsymbol{Y}$ and candidate solutions, and the second term contains an L_1 norm and a hyper parameter λ, which depends on the sparsity contribution. The greater the value of λ, the more important is the sparsity. This parameter controls whether to prioritize the reduction of the square error or the L_1 norm. For example, in matrix $\boldsymbol{A}$ (the ESD time-course images), the number of rows is the number of observation points (pixels), and the number of columns is the number of time-courses. For the analysis, the machine learning package for group LASSO[11–13]—PYTHON 3—was employed.

© Author(s) 2020

TABLE I. PCA loadings of ESD data.

PC1 (61.02%)		PC2 (7.79%)		PC3 (4.63%)	
Loading	Time of ESD data (h)	Loading	Time of ESD data (h)	Loading	Time of ESD data (h)
0.304 31	60–65	0.635 88	0–5	0.735 60	0–5
0.302 90	50–55	0.487 12	5–10	0.119 02	60–65
0.302 04	45–50	0.304 75	10–15	0.092 01	45–50
0.300 8	40–45	0.196 98	15–20	0.078 74	55–60
0.300 06	55–60	0.041 50	20–25	0.063 04	40–45
0.298 60	35–40	−0.000 51	25–30	0.062 11	35–40
0.296 89	30–35	−0.063 53	30–35	0.058 84	50–55
0.285 65	25–30	−0.089 53	35–40	−0.015 04	30–35
0.282 60	20–25	−0.168 03	40–45	−0.017 31	25–30
0.263 50	15–20	−0.198 14	45–50	−0.047 11	20–25
0.238 95	10–15	−0.206 55	50–55	−0.211 72	15–20
0.215 82	5–10	−0.212 92	60–65	−0.397 33	5–10
0.178 98	0–5	−0.239 64	55–60	−0.461 87	10–15

TABLE II. PCA loadings of fusion data.

PC1 (57.16%)		PC2 (7.62%)		PC3 (6.29%)	
Loading	Time of ESD data (h)	Loading	Time of ESD data	Loading	Time of ESD data (h)
0.3024	60–65 h	0.5363	0–5 h	0.8357	SEM
0.3010	50–55 h	0.5329	SEM	0.1155	55–60 h
0.3003	45–50 h	0.4045	5–10 h	0.0845	45–50 h
0.2990	40–45 h	0.2183	10–15 h	0.0801	60–65 h
0.2984	55–60 h	0.1450	15–20 h	0.0712	50–55 h
0.2972	35–40 h	0.0218	20–25 h	0.0544	40–45 h
0.2955	30–35 h	−0.0065	25–30 h	0.0439	35–40 h
0.2844	25–30 h	−0.0605	30–35 h	0.0286	30–35 h
0.2813	20–25 h	−0.0821	35–40 h	−0.0035	25–30 h
0.2624	15–20 h	−0.1638	40–45 h	−0.0416	20–25 h
0.2378	10–15 h	−0.1825	45–50 h	−0.1444	15–20 h
0.2154	5–10 h	−0.1980	50–55 h	−0.2463	10–15 h
0.1790	0–5 h	−0.2012	60–65 h	−0.2677	5–10 h
0.0989	SEM	−0.2130	55–60 h	−0.3301	0–5 h

E. Autoencoder

The autoencoder system by Deep Learning Toolbox for MATLAB (Mathworks, MA, USA) has three layers comprising an input layer, a hidden layer, and an output layer. Log-sigmoid was employed as a transfer function. The input data were encoded to the hidden layer to extract the essential features of the input data. The size of the hidden layer was set by an analyst. Both datasets of the ESD images and the fusion of the ESD and the SEM images were analyzed by the autoencoder, and the extracted features described in the hidden layer were compared with PCA results.

III. RESULTS AND DISCUSSION

A. Image data fusion and PCA

The ESD image of hydrogen permeating through the steel sample for 65 h was used for the image data fusion with an SEM image. The resolution of both images was adjusted to 250 × 250 pixels, and the final size of the SEM image fused with the ESD images was 316 μm (vertical) × 480 μm (horizontal). Table I lists the principal component loadings and times of the ESD data in descending order, and Fig. 1 shows the principal component score images. In the PCA results of ESD time-course hydrogen image data, the contribution ratios for principal components (PCs) 1, 2, and 3 are 61.02%, 7.79%, and 4.63%, respectively, which indicates that PC1 has the most information on the ESD data. The bright distributions in the PC1 score image in Fig. 1(a) correspond to the hydrogen distribution at the final time, and the bright distributions in the PC2 score image in Fig. 1(b) correspond to the hydrogen distribution at the initial time. Useful information was not obtained from PC3.

In the PCA results of ESD and SEM fusion data, as shown in Table II and Fig. 2, the contribution ratios of PCs 1, 2, and 3 were 57.16%, 7.62%, and 6.29%, respectively. PC1 has most of the data information as well. The bright distributions in the PC1 score

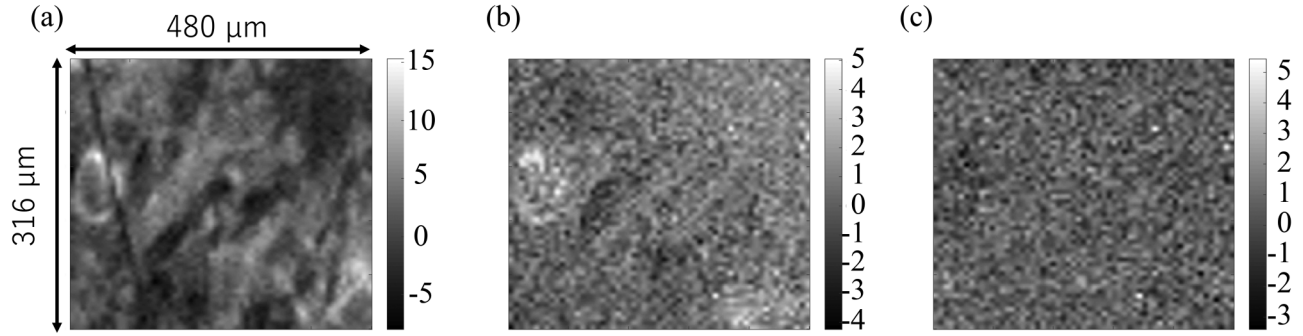

FIG. 1. PCA score images of ESD data: (a) PC1, (b) PC2, and (c) PC3. The color scale bars show the PCA scores.

© Author(s) 2020

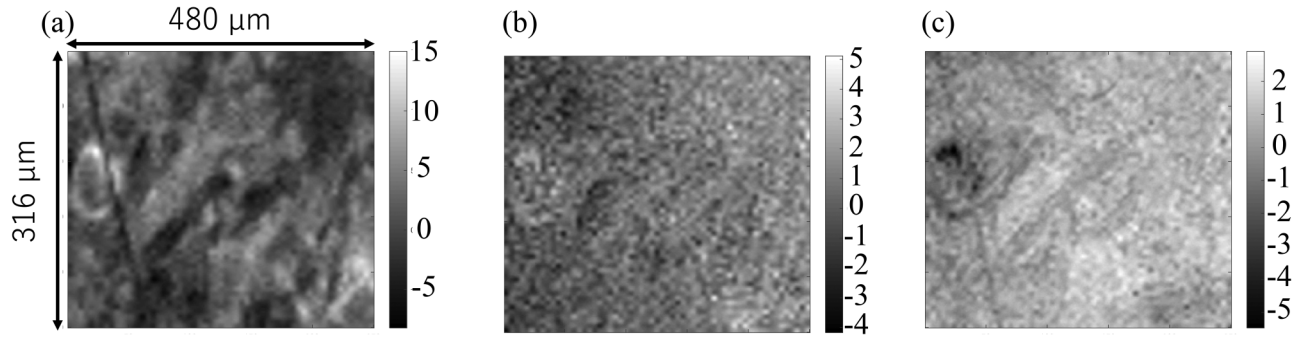

FIG. 2. PCA score images of ESD and SEM fusion data: (a) PC1, (b) PC2, and (c) PC3. The color scale bars show the PCA scores.

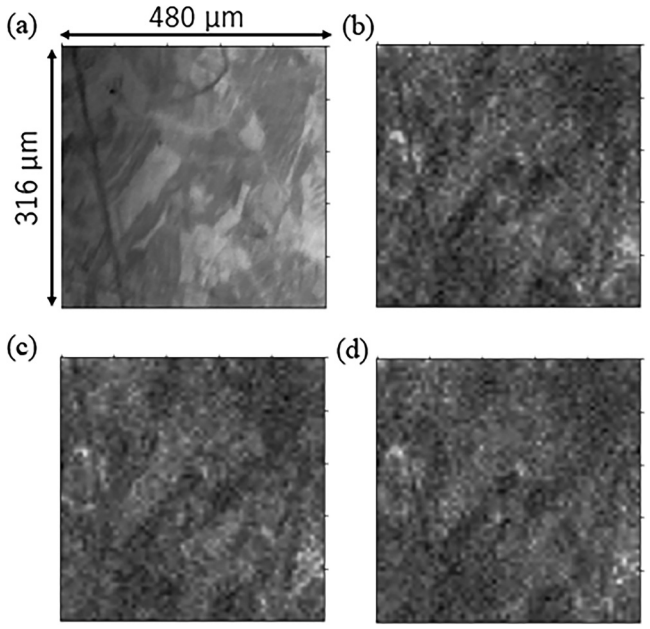

FIG. 3. SEM image (a) and hydrogen distribution images at 30–35 h (b), 35–40 h (c), and 25–30 h (d), as chosen by LASSO.

image correspond to the hydrogen distribution at the final time, the same as the PCA results of the ESD data, and the dark distributions in the PC2 score image correspond to the SEM image. The PCA score images of the fusion data have a higher spatial resolution compared with the ESD data. The bright distributions in PC2 correspond to the SEM image and the hydrogen distribution at the initial time. In PC3, the PCA score image of the fusion data has a higher spatial resolution than that of the ESD data and more useful information than that of the ESD data. The bright distributions in the PC3 score image (Fig. 2) correspond to the SEM image and the hydrogen distribution at the final time, and the dark distributions in the PC3 score image correspond to the times when the ring-shape prominently appears at the left side.

B. LASSO and autoencoder

In LASSO, the solution $\boldsymbol{Y}$ in Eq. (1) was the SEM image with a higher spatial resolution than the ESD images. The same ESD time-course images for PCA, with resolution adjusted to 250×250 pixels, were used as the data matrix $\mathbf{X}$ in Eq. (1). Group LASSO was employed in this study because a conventional LASSO method sometimes excludes some important variables. All the variables in the ESD time-course images were separately classified for group LASSO to select every single variable if necessary. When the regulation parameter λ in Eq. (1) was 2.8 and the learning rate for the gradient method was 0.03, LASSO suggested that the ESD images

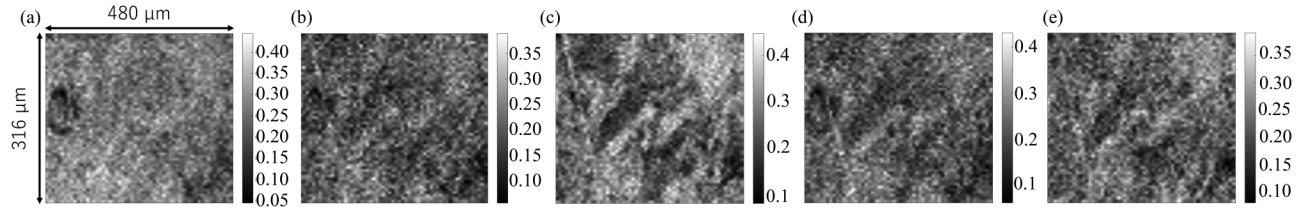

FIG. 4. Autoencoder results of ESD data: (a) encoder weight No. 1, (b) encoder weight No. 2, (c) encoder weight No. 3, (d) encoder weight No. 4, and (e) encoder weight No. 5. The color scale bars show the intensity of the encoded ESD data images.

© Author(s) 2020

TABLE III. Encoder weights for ESD data analysis by the autoencoder.

No. 1		No. 2		No. 3		No. 4		No. 5	
Encoder weight	Time (h)	Encoder weight	Time (h)	Encoder weight	Time (h)	Encoder weight	Time (h)	Encoder weight	Time (h)
0.972	60–65	1.326	55–60	0.545	10–15	0.913	35–40	0.923	40–45
0.651	45–50	0.594	25–30	0.499	5–10	0.883	50–55	0.353	25–30
0.560	50–55	0.539	40–45	0.293	0–5	0.528	55–60	0.167	35–40
−0.196	40–45	0.224	35–40	0.237	30–35	0.217	40–45	0.142	15–20
−0.249	30–35	0.039	60–65	0.220	45–50	0.129	15–20	0.133	0–5
−0.339	25–30	−0.050	20–25	0.056	20–25	−0.032	30–35	0.099	60–65
−0.346	55–60	−0.071	0–5	0.054	15–20	−0.197	10–15	0.093	20–25
−0.460	20–25	−0.319	5–10	−0.040	55–60	−0.351	5–10	0.0706	5–10
−0.491	0–5	−0.332	15–20	−0.130	25–30	−0.388	0–5	−0.164	50–5
−0.692	10–15	−0.341	10–15	−0.404	60–65	−0.423	20–25	−0.189	10–15
−0.702	15–20	−0.667	45–50	−0.459	50–55	−0.899	45–50	−0.334	30–35
−0.778	5–10	−0.782	30–35	−0.960	35–40	−1.135	25–30	−0.668	45–50
−0.821	35–40	−2.232	50–55	−1.662	40–45	−1.707	60–65	−2.158	55–60

observed in 30–35 h, 35–40 h, and 25–30 h (Fig. 3) corresponded to the SEM image. It can be inferred that in these intermediate times hydrogen was stably flowing through the steel structures, as roughly shown by SEM. This information is useful for estimating hydrogen diffusion mechanisms in a sample having multiple crystal structures.

The ESD and SEM fusion data were also analyzed using the autoencoder. Figure 4 and Table III summarize the autoencoder results of ESD data, and Fig. 5 and Table IV summarize the results of the ESD and SEM fusion data. The variables in Tables III and IV, such as time and SEM intensity, corresponding to each encoder weight were sorted in descending order. In both cases of the ESD data analysis and fusing data analysis, additional information was extracted by autoencoder than by PCA. The features of the image data were extracted with a higher spatial resolution by the image data fusion with SEM. For example, although PCA indicated the unique ring-shape hydrogen distribution on the left side of PC1 images in Figs. 1 and 2, the times specific to this distribution could not be suggested because PC1 also includes other factors. In contrast, the images of encoder weight No. 5 in Fig. 5 clearly show the ring-shape hydrogen distribution without other factors and indicate that the initial times, from 0 to 10 h, are directly related to this distribution. This suggests that hydrogen from this area permeates more rapidly than from other areas.

All trends obtained from the PCA results were also obtained using the autoencoder; however, the PCA results did not contain all information indicated by the autoencoder. For example, the factors regarding the ring-shape distribution were specified only by the autoencoder. While PCA extracted the rough features of the datasets, the autoencoder extracted additional specific features. In addition, the times corresponding to the prominent features of the sample were shown directly so that more detailed interpretation could be possible by the autoencoder.

From these results suggested by the PCA and autoencoder of the fusion data, it is evident that the image fusion data analysis can provide information on hydrogen permeation, depending on the particular structure of the steel. Although further studies are needed to characterize the detailed structure of the ring-shape area, the fusion data clearly indicate important areas for clarifying hydrogen permeation through steel. In the absence of this type of information, it is difficult to determine the areas that need to be analyzed in detail. The measurement area for the method providing nanoscale crystal structures is limited; therefore, it is important to identify important areas for further investigation.

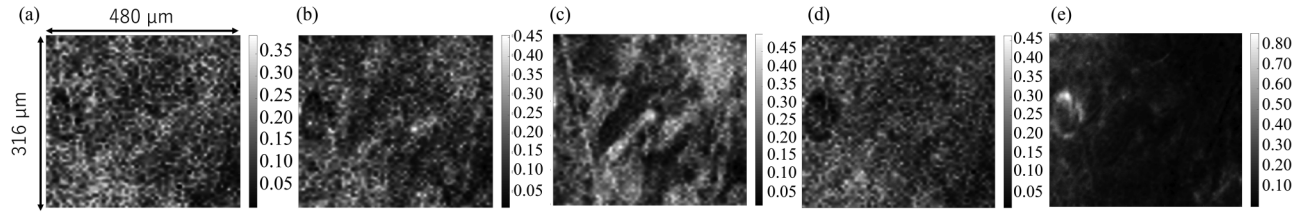

FIG. 5. Autoencoder results of ESD and SEM fusion data: (a) encoder weight No. 1, (b) encoder weight No. 2, (c) encoder weight No. 3, (d) encoder weight No. 4, and (e) encoder weight No. 5. The color scale bars show the intensity of the encoded ESD and SEM fusion data images.

© Author(s) 2020

TABLE IV. Encoder weights of ESD and SEM fusion data.

No. 1		No. 2		No. 3		No. 4		No. 5	
Encoder weight	Time (h) or SEM	Encoder weight	Time (h) or SEM	Encoder weight	Time (h) or SEM	Encoder weight	Time (h) or SEM	Encoder weight	Time (h) or SEM
1.094	5–10	1.608	5–10	1.706	10–15	0.318	55–60	0.913	0–5
0.191	10–15	1.021	0–5	0.957	0–5	0.270	60–65	0.820	5–10
0.101	15–20	0.076	45–50	0.236	15–20	0.267	50–55	0.713	10–15
−0.027	50–55	0.065	60–65	0.134	5–10	0.201	45–50	0.563	15–20
−0.042	40–45	0.044	40–45	−0.157	20–25	0.058	40–45	0.362	20–25
−0.051	55–60	−0.094	55–60	−0.195	SEM	0.025	35–40	0.353	50–55
−0.095	30–35	−0.160	50–55	−0.271	25–30	−0.059	0–5	0.306	60–65
−0.154	45–50	−0.168	35–40	−0.515	30–35	−0.086	30–35	0.280	35–40
−0.196	60–65	−0.443	30–35	−0.719	35–40	−0.099	25–30	0.276	45–50
−0.277	25–30	−0.529	SEM	−0.901	50–55	−0.183	20–25	0.259	55–60
−0.302	35–40	−0.675	20–25	−0.936	60–65	−0.294	10–15	0.256	30–35
−0.384	20–25	−0.684	25–30	−0.967	40–45	−0.844	SEM	0.217	40–45
−0.562	SEM	−0.722	15–20	−1.019	55–60	−1.071	15–20	0.186	25–30
−5.025	0–5	−3.883	10–15	−1.047	45–50	−4.549	5–10	−3.764	SEM

IV. SUMMARY AND CONCLUSIONS

In conclusion, it has been demonstrated that different types of information can be extracted depending on the data analysis method, although all the methods employed in this study, such as PCA, LASSO, and autoencoder, were useful for interpreting the time-course images of the hydrogen distribution in the steel sample obtained by the ESD. The analysis results obtained from LASSO indicated the dependence of hydrogen permeation on the steel crystal structure as shown by SEM, and the fusion data analysis by autoencoder indicated unique areas for hydrogen permeation. The image data fusion of multiple methods is powerful for the extraction of additional information, as compared to a single method.

ACKNOWLEDGMENTS

This work was partly supported by a JSPS KAKENHI (Grant No. JP 18H03849) and JST-Mirai Program (Grant No. JPMJMI18A3).

REFERENCES

[1]K. Takahashi, T. Yamagishi, S. Aoyagi, D. Aoki, K. Fukushima, and Y. Kimura, J. Vac. Sci. Technol. B **36**, 03F113 (2018).
[2]I. Rish and G. Ya. Grabarnik, *Sparse Modeling* (CRC, Boca Raton, 2015).
[3]S. A. Thomas, A. M. Race, R. T. Steven, I. S. Gilmore, and J. Bunch, "Dimensionality reduction of mass spectrometry imaging data using autoencoders," in *2016 IEEE Symposium Series on Computational Intelligence (SSCI)* (IEEE, New York, 2016).
[4]T. E. Madey and J. T. Yates, Jr, J. Vac. Sci. Technol. **8**, 525 (1971).
[5]N. Miyauchi, T. Iwasaki, T. Yakabe, M. Tosa, T. Shindo, S. Takagi, and A. N. Itakura, Appl. Surf. Sci. **492**, 280 (2019).
[6]S. J. Kim, E. H. Hwang, J. S. Park, S. M. Ryu, D. W. Yun, and H. G. Seong, npj Mater. Degrad. **3**, 12 (2019).
[7]N. Miyauchi, K. Hirata, Y. Murase, H. A. Sakaue, T. Yakabe, A. N. Itakura, T. Gotoh, and S. Takagi, Scr. Mater. **144**, 69 (2018).
[8]A. N. Itakura, Y. Murase, M. Tosa, S. Suzuki, S. Takagi, and T. Gotoh, J. Vac. Soc. Jpn. **57**, 23 (2014).
[9]G. Pimentel and S. Lozano-Perez, J. Phys. Conf. Ser. **644**, 012016 (2015).
[10]Y. Yokoyama, T. Kawashima, M. Ohkawa, H. Iwai, and S. Aoyagi, Surf. Interface Anal. **47**, 439 (2015).
[11]S. Bakin, "Adaptive regression and model selection in data mining problems," Theses sis/Library (The Australian National University, 1999).
[12]M. Yuan and Y. Lin, J. R. Stat. Soc. Ser. B **68**, 49 (2006).
[13]L. Meier, S. van de Geer, and P. Bühlmann, J. R. Stat. Soc. Ser. B **70**, 53 (2008).

© Author(s) 2020